Cement and Concrete Research 40 (2010) 1656–1663

Contents lists available at ScienceDirect

Cement and Concrete Research

journal homepage: http://ees.elsevier.com/CEMCON/default.asp

Characterisation of intra- and inter-C–S–H gel pore water in white cement based on an analysis of NMR signal amplitudes as a function of water content

P.J. McDonald *, V. Rodin, A. Valori

Department of Physics, University of Surrey, Guildford, Surrey GU2 7XH, UK

ARTICLE INFO

Article history:
Received 18 December 2009
Accepted 2 August 2010

Keywords:
B Calcium–silicate–hydrate (C–S–H)
B Microstructure
B Pore size distribution
Nuclear magnetic resonance (NMR)

ABSTRACT

^{1}H nuclear magnetic resonance (NMR) relaxation analysis of water in progressively dried white cement paste is used to estimate the width and relative specific area of intra-C–S–H sheet pores and inter-C–S–H particle gel pores. The measurement is based on the ratio of solid echo to free induction decay signal amplitudes and the observation that as water is removed, so the surface fraction contributing to the solid echo increases. The intra- and inter-C–S–H pores are found to be 1.5 nm and 4.1 nm thick respectively. The total specific area and volume ratio is 2.4 and 0.88 respectively. The volume ratio of readily evaporable water within the pore types is 0.63. Hence, the sheet porosity is 47% of the total or 38% if based solely on evaporable water. The method is distinct from NMR analyses based on the relaxation time. There is good agreement between the measured widths by the two methods.

1. Introduction

An extended series of papers have progressively explored the dynamics of water within the C–S–H gel that comprises the greater part of hydrated cement using low frequency (bench top) ^{1}H Nuclear Magnetic Resonance (NMR) [1,2]. In its most basic form, the ^{1}H NMR free induction decay (FID) signal comprises a series of discrete components with different T_2 (spin–spin) or T_1 (spin–lattice) relaxation times. The more quantitative studies are those of Lasic et al. [3,4], Miljkovic et al. [5,6], Schreiner et al. [7], Greener et al. [8], Halperin et al. [9], Bohris et al. [10] and MacTavish et al. [11]. In addition, in an important study, Plassais et al. [12] correlated magic angle spinning NMR spectroscopy results and relaxation analysis in C_3S in order to assign spin–lattice relaxation, T_1, reservoirs to different pore/chemical environments. Moreover, in recent experiments, 2D relaxation correlation and exchange methods have been employed to estimate the exchange rate between pores of different size [13–15].

Amongst the above, different studies have identified at least three T_2 relaxation components, with a minority reporting as many as five. This apparent discrepancy is in part a matter of definition. It is also in part a consequence of the experimental apparatus or method employed: not all spectrometers or all measurement protocols can detect all components. Notwithstanding these differences, it is valuable to consider carefully the water reservoirs within the cement to which each belongs. The most widely accepted assignment is as follows. The shortest lived component has a T_2 relaxation time of the order of 10 μs and originates from chemically combined water most obviously within micro-crystalline phases such as Portlandite (Calcium hydroxide, $Ca(OH)_2$ or, in cement chemistry notation CH). Longer lived signal components are assigned to gel and capillary pore water. For pore water, the fast-diffusion limit of relaxation in porous media is considered valid [16,17] in which case

$$\frac{1}{T_2^{obs}} \approx \lambda_2 \frac{S}{V} + \frac{1}{T_2^{bulk}} \approx \lambda_2 \frac{S}{V} \quad (1)$$

where λ_2 is the pore surface relaxivity and S and V are the pore surface area and volume respectively. T_2^{obs} is the observed relaxation time and T_2^{bulk} is that for bulk water. In cements and relaxation time order, the next two components have relaxation times of the order of 80–120 μs and 500 μs to 2 ms respectively. Separately resolved, these are usually assigned to “gel pore” and “capillary pore” water respectively. Any longer component is assigned to water in cracks and to water adsorbed on the sample surface. Assignment of water between the sheets of the calcium silicate hydrate (C–S–H) gel is less clear. It is sometimes considered NMR similar to the chemically combined water; sometimes it is considered like gel pore water. This mirrors a wider debate in the cements literature as to the characteristics of gel water and the detailed morphology of the microstructure of C–S–H.

The purpose of this paper is to carefully examine the amplitude of the solid and more mobile T_2 relaxation time components in cement pastes with a view to confirming the detailed assignment of relaxation components to cement microstructure. Measurements are made as a function of sample moisture content during careful, and ultimately destructive, drying starting with a few minutes heating at a few degrees above ambient temperature and ending at temperatures of the order of 400 °C for several hours. The NMR measurement is accomplished by measuring the amplitude of the shortest relaxation time fraction using a solid echo experiment [18] combined with FID

* Corresponding author.
E-mail address: p.mcdonald@surrey.ac.uk (P.J. McDonald).

0008-8846/$ – see front matter © 2010 Elsevier Ltd. All rights reserved.
doi:10.1016/j.cemconres.2010.08.003

intensity analysis. The amplitude of each T_2 relaxation component is directly proportional to the fraction of water, or, more strictly ^{1}H in a corresponding reservoir. By this method we seek to more carefully assign especially the shortest relaxation time components to water in different environments. While presence of inter-pore water exchange may modify the relative amplitudes of the longer components individually considered, it has minimal effect on the relative amplitude of the chemically combined water signal and the aggregated mobile water signal as measured here.

A by-product of the study has been the realisation that the NMR intensity measurement leads to an alternate assessment of the gel pore size based not on the absolute value of the more mobile component T_2 through Eq. (1), but rather on the amplitude of the "solid" and "mobile" component as a function of moisture content. It is also possible to calculate the ratio of the pore specific areas and volumes. The measurements derive from the observation that, during the early stages of drying during which easily evaporable water is lost, not only does the fraction of bound water increase, but so does the absolute volume due to the increasing presence of a residual adsorbed layer. The analysis also sheds some light on the means of drying of these pores. The new methodology for measuring pore size has an advantage compared to that based on the use of Eq. (1) because it is calibration independent, meaning that the surface relaxivity λ is not required to calibrate the experiment.

Current literature presents a series of potential models for the microstructure of cement gel, reflecting the ongoing debate as to the morphology of C–S–H and related phases. These models are based on the interpretation of data arising from different spectroscopies and imaging methods including neutron and X-ray scattering, electron microscopies and magnetic resonance. At issue is the scale of the heterogeneities within the microstructure, the morphology of the C–S–H sheets and the extent to which elements of C–S–H may, or may not, be viewed as discrete particles. Many of these models have recently been reviewed by Jennings [19]. The results of this work are discussed in the context of a model proposed by Feldman and Sereda [20] which is the model towards which most prior NMR work by our group has been pointing. It is possible, however, to see how the results, which offer insight into pore size, could be re-interpreted in terms of other models. This is discussed further in Section 6.1.

The key observation of this work will be that the apparent bound water fraction changes in a non-intuitive manner as cement samples are dried and that this leads to a new estimate of pore size. Indeed, two characteristic pore sizes are calculated. The numerical results are generally in agreement with other estimates made by other means. However, the exact values obtained may be questioned due to the manner of sample drying which is in a vacuum oven up to 200 °C and an ordinary oven beyond. Carbonation and microstructural damage both play a role. The likely impact of this, and mitigating factors, is discussed in Section 6.2. Neither microstructural damage nor carbonation invalidates the measurement of bound water fraction as measured by NMR in as cured material that was the original driver of this work.

2. Experimental

2.1. Materials

White cement was obtained from the European NANOCEM consortium materials bank (Nanocem Cement "A") developed as part of the Nanocem Marie Curie Project [21]. It was used in all experiments. The composition is known to be 67.3% Alite, 23.3% Belite, 3.6% Aluminate and 4.3% Gypsum/Hemihydrate/Anhydrite with other phases less than 1.5% total. Carefully measured amounts of the cement powder were mixed in the water to cement ratio of 0.4 at room temperature according to the NANOCEM protocols: in summary mix for 3 min at 500 rpm, pause for 2 min, then re-mix for 2 min at 2000 rpm. The cement was cast in cylindrical moulds 8 mm in diameter and 20 mm deep. Once set, the samples were removed from the moulds and cured under a small quantity of saturated calcium hydroxide solution at room temperature. The curing time was variously 2, 4 or more weeks. After curing, and immediately prior to use, samples were dabbed dry, ground in a pestle and mortar to a coarse grain and placed in 10 mm diameter NMR tubes. Care was taken to ensure that the sample fitted well within the NMR sensor to avoid fringe effects. Measurements were made on progressively dried samples. A vacuum oven was available up to 200 °C and an oven without vacuum beyond that to 450 °C although the maximum temperature reported here is 380 °C. Samples were weighed at every opportunity: before and after both measurements and periods of drying. All measurements were made at room temperature, not at the drying temperature. Reagent grade calcium hydroxide upon which parallel experiments were carried out was purchased from Sigma-Aldrich.

2.2. Methods

^{1}H NMR data was acquired using a Resonance Instruments "Maran" bench top NMR spectrometer (Oxford Instruments, Whitney, Oxon UK) operating at 20 MHz. The solid echo pulse sequence, $90_x\ \tau\ 90_y$ acquire, where $90_{x/y}$ is a 90° excitation pulse of relative phase x or y and τ is a short delay interval was employed. The precise timing diagram is shown in Fig. 1. Following the second pulse and a short instrument dead time (≅10 μs) the solid echo and free induction decay signal were detected. Dependent on signal level, up to 2048 averages of 1024 points per decay were acquired with a recycling time of 1 s and at a sampling rate of 1 MHz respectively. Echoes were acquired for pulse gaps, τ, from 15 to 45 μs in 5 μs intervals. In all cases a small residual NMR signal emanating from the empty NMR probe was subtracted from the measured data and all acquisitions were normalised by the number of averages.

2.2.1. Data analysis

The signal from mobile hydrogen following the $90_x\ \tau\ 90_y$ pulse sequence is unaffected by the second pulse and is therefore an exponential decay with apparent origin at the time of the first pulse and relaxation time, T_2^*, that is determined by the magnet inhomogeneity. In contrast, Powles and Strange [18] have shown that, for rigid coupled spin 1/2 (i.e. hydrogen) pairs such as in solid $Ca(OH)_2$, the pulse sequence refocuses magnetisation that would otherwise decay rapidly due to rigid dipole–dipole interactions so that the signal from the solid comprises an echo of approximately Gaussian shape centred on a time τ after the second pulse. Hence, the composite signal can be approximated by, and fit to

$$I(t,\tau) = I_m(\tau)\exp\left(-\frac{(t+\tau)}{T_2^*}\right) + I_s(\tau)\exp\left(-\left(\frac{t-\tau}{\sigma}\right)^2\right) \quad (2)$$

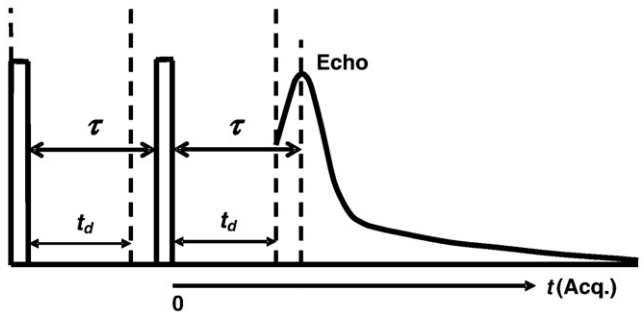

Fig. 1. The solid echo pulse sequence timing diagram.

where I_m and I_s are the mobile and solid intensities respectively, σ is the Gaussian width (approximate solid T_2) and t is time from the second pulse.

The echo refocusing is not total due to longer range interactions and residual motion. Therefore, to obtain a true measure of the solid intensity it is necessary to back extrapolate $I_s(\tau)$ to $\tau=0$. This has been done using linear, exponential and Gaussian fitting. Empirically, the exponential was found to fit the data best and it is these results that are reported below. For completeness and to overcome residual errors, $I_m(\tau)$ was also back extrapolated.

3. Theory

The much simplified model of cement microstructure adopted in this work follows closely that of Feldman and Serada [20]. This structure is suggested in Fig. 2e. We consider that cement gel is composed of tetrahedral silica layers interspersed by layers of water and calcium ions in a sheet like structure. For clarity, we refer to this water as intra-C–S–H sheet water. The C–S–H sheets are randomly stacked with water in inter-C–S–H gel pore spaces. While many authors would refer to water in both reservoirs as "gel water", we maintain the above distinction throughout to avoid ambiguity. Water in both intra- and inter-C–S–H sites may be considered as being confined to planar pores. We include within this description other comparably structured phases such as AFm and Ettringite. In addition there are solid phases such as Portlandite.

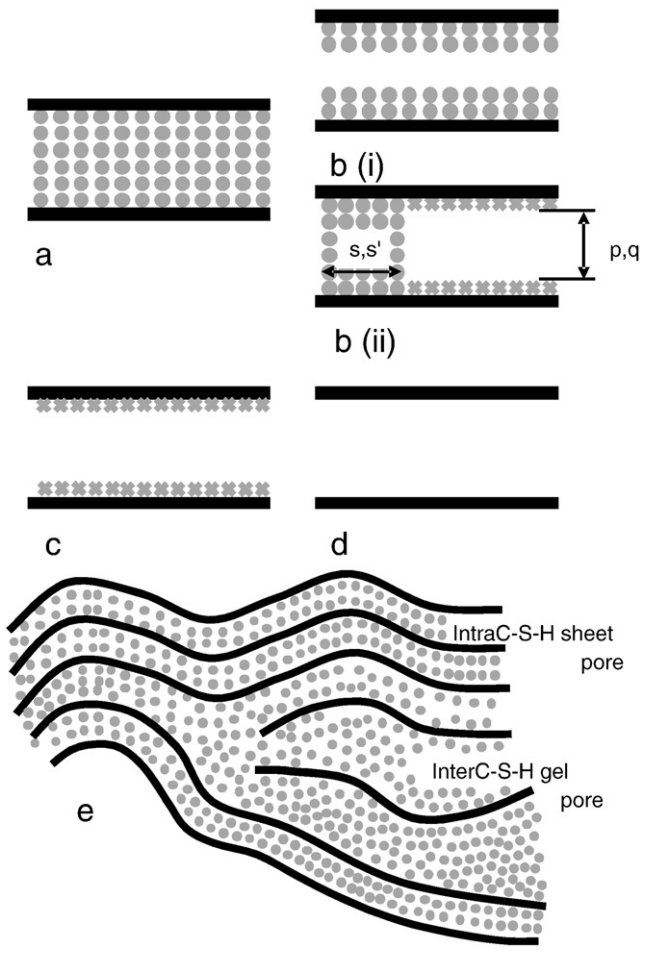

Fig. 2. (a) A planar pore full of mobile water (circles). (b) Two possible ways of emptying a pore showing mobile and immobile (crosses) water. In (b(ii)) definitions of p (and q), and s (and s') are shown. (c) A pore with surface adsorbed water only. (d) An empty pore. (e) An illustrative schematic defining intra-C–S–H sheet and inter-C–S–H gel pore water (after Ref. [20]).

Consider a planar pore as suggested in Fig. 2a. In this pore, the water molecules associated with the surface are in rapid exchange with those in the bulk of the pore. Hence they are characterised as mobile and the NMR signal has a long relaxation time. Fig. 2d shows the pore completely dried, with no water remaining. There will be no signal. Fig. 2c shows an intermediate stage of drying where all the readily evaporable water has been removed and the remaining water is adsorbed to the surface. It is relatively immobile and so has a short relaxation time. Fig. 2b(i) and 2b(ii) illustrates two alternate drying scenarios leading to Fig. 2c. In Fig. 2b(i), water is removed uniformly across the pore. The surface to volume ratio of the remaining water is increasing so that, from Eq. (1), T_2 is decreasing. However, the T_2 distribution remains unimodal. The scenario of Fig. 2b(ii) arises if capillary forces are significant. Here there is a clear demarcation of the T_2 distribution corresponding to a component with the original relaxation time but decreasing amplitude, and a second short relaxation time component with increasing amplitude.

Suppose that, for an as prepared sample, the total specific area of inter-C–S–H gel pore water measured in surface water molecules per unit volume of C–S–H is M and that a typical inter-C–S–H gel pore is $(p+2)$ water molecules thick. The model is insufficiently precise to warrant distinction between water molecules adsorbed to pore surfaces and surface hydroxyls. Then the signal intensity due to the inter-C–S–H gel pore water is proportional to $M(p+2)$. A similar argument can be composed for the intra-C–S–H sheet water save here we have a specific area of N surface molecules per unit volume and write the water layer thickness as $(q+q')$ molecules. We use q' rather than 2, since, as water is removed, residual water associated with the calcium ions may appear as bound. The signal intensity due to the intra-C–S–H sheet water is proportional to $N(q+q')$. Finally, we assume that the signal intensity due to the CH is proportional to Lr where L and r are an effective CH surface area per unit volume of C–S–H and an effective CH thickness respectively. Normalising to unity, the total initial signal intensity is

$$M(p+2)+N\left(q+q'\right)+Lr=1 \tag{3}$$

The pore water is in fast exchange with the surface adsorbed water and appears as mobile. The CH water is bound and solid like. Thus, the initial intensities for the mobile (I_m) and solid (I_s) signal intensities back extrapolated to $\tau=0$ are given by

$$I_m = 1-I_s = M\cdot(p+2)+N\cdot\left(q+q'\right)=1-Lr \tag{4}$$

Consider now that the pores are dried according to the schematic Fig. 2b(ii). Evaporable water is removed from a fraction $(1-s)$ and $(1-s')$ of the specific area of the inter-C–S–H gel and intra-C–S–H sheet water leaving an upper and lower surface mono layer in the former case and a total q' molecules per unit area in the latter. Once the evaporable water is removed, the remaining water that was in fast exchange is immobilised and joins the "solid" fraction. Hence, during drying

$$I_m = M\cdot(p+2)\cdot s+N\cdot\left(q+q'\right)\cdot s' \tag{5}$$

and

$$I_s = 2M\cdot(1-s)+q'N\cdot\left(1-s'\right)+Lr \tag{6}$$

The normalised mass of water remaining during drying is:

$$\rho = 1-Mp\cdot(1-s)-Nq\cdot\left(1-s'\right) \tag{7}$$

Experimental evidence to be presented suggests that the drying is characterised by three distinct stages. It is assumed that the first stage corresponds to removal of evaporable water from the inter-C–S–H gel pores only. Hence, during the first stage, $s'=1$, leading from Eqs. (5) and (7) to

$$I_{m1} = a_1\rho + b_1 \tag{8}$$

where I_{m1} is the stage 1 mobile intensity and

$$a_1 = 1 + \frac{2}{p} \text{ and } b_1 = M\cdot(p+2) - \frac{2}{p} + N\cdot\left(q + q'\right) - 1 \tag{9}$$

Eq. (8) characterises the mobile signal intensity as function of mass during early drying. The relationship is linear, with gradient a_1 and intercept b_1. The second stage is assumed to correspond to removal of evaporable water from the intra-C–S–H sheets. During this stage, $s=0$ and $s'<1$ so that, using similar notation to above

$$I_{m2} = a_2\rho + b_2 \tag{10}$$

with

$$a_2 = 1 + \frac{q'}{q} \text{and } b_2 = Mp + \frac{q'}{q}\cdot(Mp-1) + N\cdot\left(q + q'\right) - 1 \tag{11}$$

The model parameters p, q and M and N can be calculated from Eqs. (9) and (11) as:

$$p = \frac{2}{a_1 - 1} \tag{12}$$

$$q = \frac{q'}{a_2 - 1} \tag{13}$$

$$M = \frac{\frac{2}{p} - \frac{q'}{q} + b_1 - b_2}{2 - p\frac{q'}{q}} \tag{14}$$

$$N = \frac{\frac{q'}{q} - Mp\cdot\left(1 + \frac{q'}{q}\right) + b_2 + 1}{q + q'} \tag{15}$$

The product Lr is available from the solid signal intensity before drying although nothing can be said about the L and r separately, that is the shape of the CH crystals.

The final stage of the drying, that only occurs with more extreme heating, is removal of the "solid" water. It is broken down into at least two processes. The first is removal of surface adsorbed water both from intra-C–S–H sheet and inter-C–S–H gel pores. The second is water lost due to breakdown of CH into C + H; that is $Ca(OH)_2$ into CaO and water.

A further process that is not "drying", but which materially affects the results, is carbonation of the C–S–H and CH. Carbonation involves the ingress of CO_2 such that

$$Ca(OH)_2 + CO_2 \rightarrow CaCO_3 + H_2O$$

And

$$C_xS_yHz + xCO_2 \rightarrow xCaCO_3 + ySiO_2\cdot tH_2O + (z-t)H_20$$

The ingress of CO_2 causes an increase in net mass even though there is a loss of signal due to loss of water.

4. Results

We consider first the inset to Fig. 3. This shows a solid echo signal measured from dried and powdered reagent grade $Ca(OH)_2$. In this measurement, $\tau = 20\,\mu s$. The echo is seen to decay rapidly and to be followed by a small negative going oscillation known as a Pake doublet. Pake doublets are a well known feature of systems comprising rigid pairs of dipolar coupled spin 1/2 nuclei such as hydrogen protons in $Ca(OH)_2$ [22].

The main part of Fig. 3 shows an exemplar echo signal recorded from a cement paste sample. The sample has been dried progressively at temperatures up to 120 °C and at this stage has attained a fractional mass compared to the start of 0.80 so that most of the evaporable water has been lost. Moreover, the pulse gap τ is 40 μs which is relatively long, so the solid echo is already significantly attenuated. Hence, the signal to noise ratio of this measurement is relatively low at 15. It is therefore close to a "worst case" data set from the viewpoint of data analysis. Nonetheless, the signal can be well fit to an exponential decay and a Gaussian according to Eq. (1). The relaxation time fit parameters are $\sigma = 18.3$ and $T_2^* = 71\,\mu s$ for the bound and mobile components respectively. The corresponding signal amplitudes are 5.85 and 9.00 respectively.

Fig. 4 shows the pulse gap dependence of the echo and decay fit amplitudes for the cement sample at the same drying conditions as in Fig. 3. It is seen that the bound signal amplitude is a strong function of the pulse gap whereas the mobile signal amplitude is a much weaker function. Both amplitudes have been fit to single component exponential decay curves as a function of the pulse gap and back extrapolated to zero time in order to gain the best estimate of the bound and mobile hydrogen fractions. In this example the amplitudes at zero time are 48.3 (bound) and 8.2 (mobile).

Fig. 5 shows the amplitude of the bound and liquid signals and their combined total as a function of the sample mass. All signal amplitudes have been normalised to the overall initial total (solid + mobile) amplitude and are therefore fractions. The sample mass is shown in 3 ways. The primary axis shows the actual mass of the sample relative to the initial mass. It is seen that the sample dries to 77% of the starting value at the maximum temperature attained. The subsidiary second and third axes immediately below, show the relative water fraction based on knowledge of the sample composition at mixing, and of the curing and preparation conditions. They are discussed below. The axis above the plot shows the maximum drying temperature used to reach the corresponding sample masses. This is indicative only of the temperature required since, to a limited extend, the same mass can be achieved by a longer drying period at lower temperature or, conversely shorter period at higher temperature than actually used.

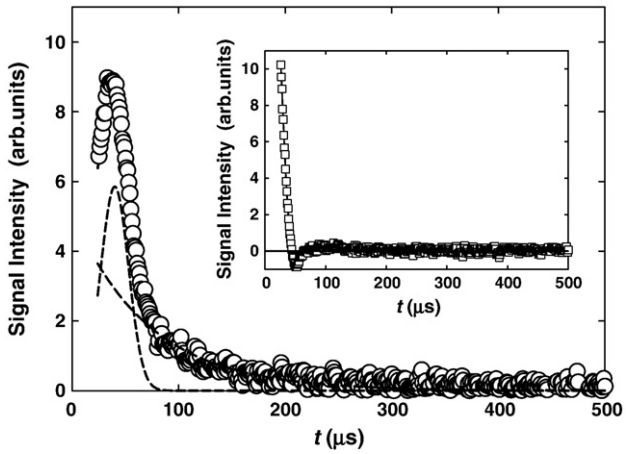

Fig. 3. An exemplar solid echo signal ($\tau = 40\,\mu s$) recorded from white cement paste after drying to 0.80 the initial mass. Inset: a similar echo ($\tau = 20\,\mu s$) from dried $Ca(OH)_2$. The dotted lines show the Gaussian and free induction decay signals fit to the data. The Gaussian is centred on $t=\tau$; the decay is extrapolated back to $t=-\tau$ (not shown). A solid line, almost totally overlain by data points, is the combined fit.

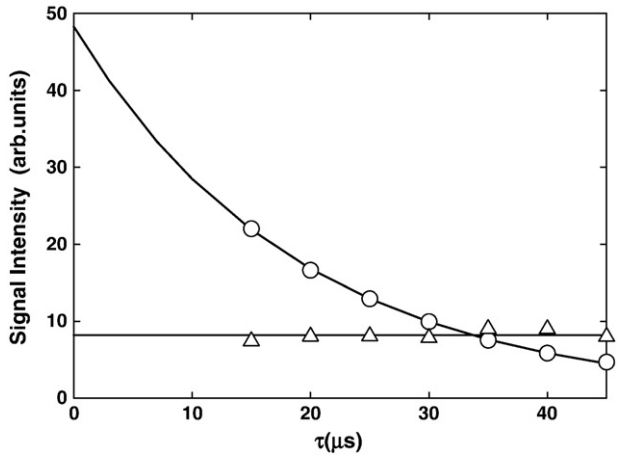

Fig. 4. The τ dependence of the solid echo (circles) and mobile (triangles) signal intensity for white cement paste after drying to 0.80 the initial mass. The solid lines are exponential decay fits to the data.

This experiment has been repeated on several samples, albeit not always with as many data points. The essential features to be discussed in the next section are highly reproducible.

5. Analysis

5.1. Initial observations

The primary observation to be made from the inset to Fig. 3 is that we are satisfactorily working in a regime where we can see the broadest line components as evidenced by observation of the Pake doublet for $Ca(OH)_2$. For cement, the echo is clearly partitioned into two components reflecting the bound and more mobile water.

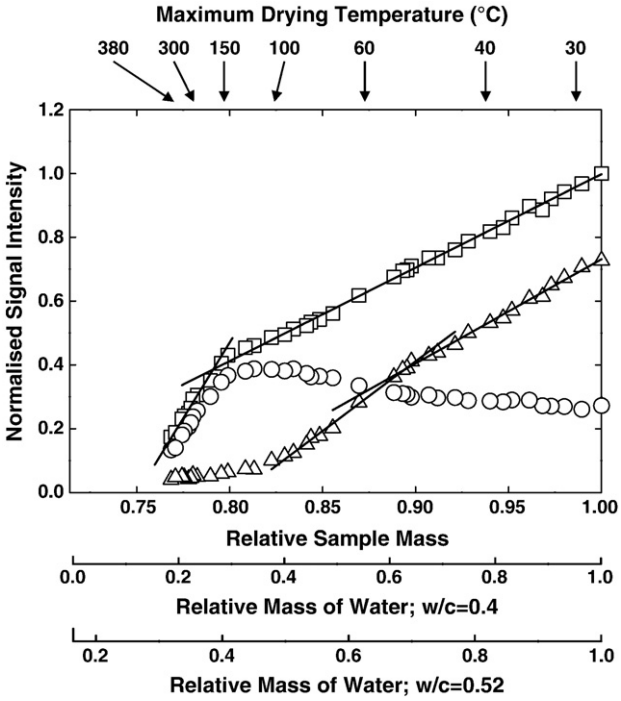

Fig. 5. The total NMR signal (squares), solid (circles) and mobile (triangles) signal fractions as a function of the actual relative mass of the sample (top axis); of the relative mass of water assuming a water to cement ratio of 0.4 (middle axis); and of the relative mass of water assuming a water to cement ratio of 0.52 (bottom axis). The indicative drying temperature is shown above the plot. The solid lines are least squares fits to the data discussed in the text.

Interestingly, the same is true for as-received $Ca(OH)_2$ which clearly holds a significant fraction of adsorbed water on the crystallites. The inset is for dried material. The mobile water signal in the cement is not differentiated into different reservoirs with different T_2 values reflecting different pore size environments because the experiment is magnet inhomogeneity (T_2^*) limited. As a result, any amplitude and T_2 modification resultant from exchange between pores of different size is not affecting the result.

The second observation (confirmed by an NMR Carr–Purcell–Meiboom–Gill [23] analysis as used in our previous work) is the almost total lack of a very long T_2 component that might be attributed to large capillary pore water. When present, water in large pores should manifest as a long T_2 component to the signal. This perhaps surprising result is not new. Previous NMR data on similarly prepared samples of white cement with a water to cement ratio of 0.4 prepared in our laboratory have also exhibited almost no capillary pore water despite the samples being cured underwater [13]. A similar observation has been made by others. For example, Halperin et al. [9] report pores of characteristic size of circa 3 and 12 nm, but nothing larger, in mature pastes on the basis of NMR T_2 relaxometry. Larger pores (>100 nm) are only seen in the first few hours of hydration.

The first conclusion to be drawn from Fig. 5 is that, initially, 27% of the signal is in the solid fraction and 73% in the mobile. It is suggested that, at this stage, the bound fraction is made up exclusively from signal from the CH: the Portlandite. The cement pores are fully saturated and the pore water hydrogens, if not the water molecules themselves, are in rapid exchange with water and hydroxyls occupying the pore surface. Hence all the C–S–H water appears as mobile.

As water is removed from the sample, so the total signal decreases. The decrease is linear in two distinct regions with different gradients: first in the relative sample mass range 1.0 to 0.8 and then with a strongly accelerated gradient below 0.8. More careful inspection of the bound and mobile fractions in the range 1.0 to 0.8 mass fraction suggests that the first part itself divides into two stages. Hence we refer to three stages of drying: the first and second from 1.0 to 0.8 mass fraction and the third below 0.8.

Linear signal loss with mass is expected as each lost water molecule contributes equal signal: hence the observation of accelerating signal loss below 0.8 mass fraction in stage 3 is a surprise, discussed further below. For the present we confine discussion to the behaviours between 1.0 and 0.8. In this range, it is reasonable to expect that readily evaporable water is lost. One therefore expects the mobile fraction to decrease in parallel with the total. In fact, it decreases more quickly while the bound fraction increases.

This is better understood with reference to the second and third axes which show the sample mass in terms of the calculated water content. Given that the water to cement ratio is 0.4, unity water fraction on the second axis corresponds to an actual water content of 28.6%: equally, 0 corresponds to a relative sample mass of 71.4%. Based on the second axis, the gradient of the total water signal loss curve is 0.836. This is close to, but not equal to, the expected value of 1.0. The reason is almost certainly due to error in the water fraction calculation. The sample was prepared with a water to cement ratio of 0.4, but was subsequently cured under a saturated calcium hydroxide solution. Since the sample is small, any water ingress raised the water to cement ratio of the final product. Equally, the cured sample was crushed in air before use and likely dried slightly. In principle, both effects can be quantified gravimetrically. In practice, residual bulk sample surface water and sample losses on crushing make this difficult. Notwithstanding, a correction can be carried out within the analysis. However, looking forward to what follows, we note that applying this correction does not substantially affect the quantitative conclusions of the work. The correction adopted first is to change the effective water to cement ratio in order to force the gradient of the best fit line to the total signal loss relative to the calculated water

fraction to be equal to 1.0 down to a sample mass fraction of 0.8. The effective water to cement ratio required to achieve this is found to be 0.52. This is the basis of the third axis presented in Fig. 5 and, unless otherwise explicitly stated, all further discussion refers to this axis.

5.2. Readily evaporable water, pore size and porosity analysis

The mobile fraction decreases linearly between water fractions 1.0 and circa 0.75. We refer to this as the first stage of drying. Below 0.75, the mobile fraction starts to decrease at a slightly faster rate before plateauing out close to zero. This is the second stage. The bound fraction increases in sympathy with the mobile fraction decrease while mobile signal remains. Thereafter, it decreases sharply towards zero in the final third stage of drying as previously noted. There are therefore two clear stages of loss of evaporable water. We seek to employ the model embodied by Eqs. (3)–(15). To that end, we have fit the mobile water loss to a straight line function first in the range 1.0 to 0.74 (stage 1, axis 3) and then again in the range 0.69 to 0.57 (stage 2, axis 3). Fig. 5 shows the best fit lines. In stage 1, the gradient and intercept are 1.16 and −0.424 while in stage 2 they are 1.60 and −0.717. Direct application of the model, and assuming $q'=2$ representing a mono layer of adsorbed hydrogen in the sheet pores yields pore thicknesses of $(p+2)=14.6$ water molecules and $(q+2)=5.3$ water molecules for the two pore types respectively.

Given no NMR evidence for large capillary pores, we assume that the first pores to dry are the inter-C–S–H gel pores and infer that these have a nominal width of 4.1 nm on the basis of 0.28 nm per water molecule [24]. Equally, we assume that the next (second) stage of drying involves water loss from the intra-C–S–H sheet pores in which case these have a width of 1.5 nm. The larger of these two widths, which are calculated from the *amplitudes* of the NMR signal, is a little below, but generally in accord with, the estimated range of our previous results which were based on the NMR relaxation *time*s [13,14]. The smaller is fractionally larger than that previously estimated. Both methods assume fast exchange of hydrogen between pore surface and bulk sites. The relaxation time method however, requires considerable reliance on careful calibration of the pore surface relaxivity: detailed model dependence that is not inherent to the new estimates. Moreover, the new analysis goes further than the previous analysis based on relaxation times in so much as the relative specific surface area of the two pore types can also be evaluated. The intercepts of the fit lines in Fig. 5 can be used in conjunction with Eqs. (12)–(15) to yield $M=0.027$ and $N=0.065$ both in arbitrary signal intensity units. The ratio, N/M is the ratio of the specific area of intra-C–S–H sheet to inter-C–S–H gel pores respectively. This ratio is 2.4. As a guide, if it is assumed that gel pores arise from the arbitrary stacking of layers of a few sheets each, then they will likely have a comparable area. Hence one may conclude that the C–S–H layers are on average 2 to 3 sheets thick.

Also, one can calculate the ratio of the sheet to gel porosity as $N(q+2):M(p+2)=0.88$. This implies that the sheet porosity is 47% of the total. However, if the porosity is based on the easily evaporable water content only, then the volume ratio is $Nq:Mp=0.63$ so that the sheet porosity is 38% of the total.

5.2.1. Alternate corrections to data

These calculations have been based upon a calculated effective water to cement ratio of 0.52. The alternate correction factor is to add a constant to the sample mass to reflect water loss during crushing, again to force the gradient of the total signal loss to unity. The necessary correction factor required is −29.9% of the water content at w/c = 0.4. This is negative suggesting that the sample gained water from the air during crushing. This is unrealistic. Notwithstanding, the fit parameters for this correction yield $(p+2)=14.6$ and $(q+2)=5.3$. These are both unchanged reflecting the pore thickness model invariance to these corrections. The pore specific areas are more affected: $M=0.011$ and $N=0.084$ giving pore areal and volume (porosity) ratios of 7.6 and 2.8 respectively. A difficulty with this correction is that the predicted Portlandite fraction becomes 39%.

A further enhancement to the fitting is to not only force the gradient of the total signal loss to unity, but also require the Portlandite fraction to be the 28.8 based on XRD analysis of samples made from the same material by similar methods [25]. This is achieved for an effective water to cement ratio of 0.49 and a crushing water mass gain of 6%. In this case $(p+2)=14.6$ and $(q+2)=5.3$ as before and $M=0.024$ and $N=0.068$ so that the sheet to gel pore area and volume (porosity) ratios are 2.8 and 1.0 respectively in reasonable agreement with the earlier estimate based on a water to cement ratio correction only.

5.3. The third stage of drying

Finally we explore the third stage of drying. Here we find that, after a transition around 180 °C, relative sample mass circa 0.8, we see a greatly accelerated loss of total signal with mass. Unfortunately this coincides with our need to switch to a non-vacuum oven at 200 °C. The graph is near linear with a gradient of 3.0 (axis 3). Since signal is lost in direct proportion to water loss in the readily evaporable stages, the only possibilities are that to a greater or lesser extent, hydrogen, but not oxygen is being lost or that the sample is also gaining mass in parallel with drying. We look to carbonation as a mechanism for the latter. Differential scanning calorimetry (DSC) experiments performed on duplicate samples showed that carbonation is indeed significant on our completely dried material, although it is not possible to exactly quantify the extent from the DSC carried out. Given the molecular mass of water (18) and carbon dioxide (44), we calculate that the observed total signal loss with mass is achieved if, for every water molecule leaving the sample, 0.273 CO_2 are gained. Put another way, we gain 1 CO_2 for every 3.66 waters lost. Up to a temperature where the bound intensity re-attains the initial value, it is reasonable to assume that this is carbonation of the C–S–H. This would be in accord with conventional understanding where carbonation accelerates in partially dried C–S–H [26]. Such an analysis and interpretation then suggests that there are circa 3–4 evaporable water molecules associated with each Ca ion if complete carbonation is achieved. However, since this is stage 3, the implication would be that $q'>2$ in stage 2. The apparent discrepancy is almost certainly an artefact of assuming discrete drying stages.

Beyond a temperature of 180 °C the experiment begins to enter a regime where breakdown of the Portlandite into C and H is possible and where carbonation of the C within Portlandite can become significant. Hence the total signal decreases below the initial bound value.

6. Discussion

6.1. C–S–H microstructure

Taylor [27] reviews work and presents further data on the water content of cement, discussing this in the context of evaporable/non-evaporable water (non-evaporable being defined as that remaining at circa 150 °C) and bound/unbound water (bound being defined as that remaining at circa 90 C or 11% RH). He presents exemplar calculations of mass balance and water content for different cement phases from which the bound and non-evaporable water fractions are calculated, noting that “many variants of the calculation are possible” [27]. Observing the difference between bound and non-evaporable water contents, the conclusion is reached that the Feldman–Sereda model [20] is compatible with “the essential features” of the Powers–Brownyard model [28] and that “about a third of the gel porosity of the Powers Browyard model is inter layer space” [27] — that is intra-

C–S–H sheet as defined in this work. Our results support these calculations and observations.

In a series of papers based on the results of small angle neutron and X-ray scattering, Jennings, Allen and co-workers [19,29,30] have proposed a hierarchical structure comprising highly concentrated, colloidal C–S–H nano-particles dispersed in water. The particles are made of sheet like solids interspersed with water layers as discussed here. The particles pack and flocculate into what they term "globule flocs" producing further gel pores with characteristic sizes 1–3 and 3–12 nm. The primary differences to the analysis presented here are that, first we consider a hierarchy of only two sizes and second that we consider that the inter-particle pores are predominantly planar. It is possible to modify our analysis for the case of spherical particles. If this is done, then, in order to obtain the same surface to volume ratio for the space between the particles, the radius of the particles should be 6.7 or 5.2 nm depending on whether cubic or hexagonal packing is assumed. Considering the wide range of sizes proposed the results presented in this paper are not incompatible.

In other work, Richardson [31] discusses a distinction between high density inner product and low density outer product. The outer product is further dependent on the C/S ratio, being either fibrillar or foil like. The proposed geometries are more consistent with the suggestions of this work, although without considerably more data on different cements, at different ages and at different C/S ratio, we cannot resolve the finer distinctions of Richardson.

More recently, Pellenq et al. [32] have carried out molecular dynamics simulations of C–S–H starting from tobermorite–jennite like structures in which the C/S ratio has been adjusted and the water content slowly relaxed to equilibrium. This results in a sheet structure with a C–S–H density much closer to that measured by small angle scattering, distorted layers around the silica regions and a modified sheet spacing with additional adsorbed water. The spacing is not too far removed from the 1.5 nm calculated in this work. The adsorbed water is found to be in ultra-high confining environments. Pellenq et al., however, did not comment on the size of the larger pores between C–S–H particles.

6.2. Carbonation and microstructural damage

Two potential criticisms of our work are first that the sample was dried by heating and second that the experiments were not performed in a CO_2 free environment. The former, especially drying at elevated temperature, almost certainly led to microstructural damage. The latter led to carbonation. The reasons are both historical and pragmatic. The initial aim was only to ascertain the bound water fraction in as cured material as measured by NMR in order to compare this with expectation. For this reason, neither subsequent damage by heating nor carbonation was an issue at the outset. Only subsequently, was it realised that the data potentially contained new pore size information and that the significance of this information was likely greater than the initial result, but that carbonation and damage due to sample preparation were therefore problematic.

We discuss the likely impact of carbonation on the results first. Up to a temperature of 200 °C, the samples were dried in a vacuum oven and measured at room temperature in small sealed tubes. This will have lessened opportunity for carbonation. That it is not hugely significant is suggested by the fact that the gradient of total signal loss with mass in Fig. 5 is constant and, for the uncorrected relative mass axis, a little less than one. Carbonation would have increased the gradient above one. Also, over such a wide mass loss range, one might not expect the degree of carbonation to always be proportional to the total mass loss (especially given the mode of drying in short bursts) as would needs be the case for a linear decrease. Since all the pore size information is calculated from well within this range of drying temperature, then we believe that the pore sizes deduced are more reliable than simply indicative.

Above 200 °C, a vacuum oven was not available. The signal loss gradient increases dramatically due to carbonation as discussed. No pore size information is deduced here. Rather, an estimate is made of the degree of carbonation in terms of the number of added CO_2 for total lost water molecules. That carbonation has occurred is further evidenced by the DSC experiments performed on the dried material.

We turn now to the impact of microstructural damage due to heating. Potentially this is a more serious problem as it negates one of the primary advantages of NMR which is usually regarded as both non-destructive and non-invasive. Not even drying by other means will necessarily overcome this difficulty. However, careful consideration of the effect that collapse of empty pores may have on our results suggests that the impact may not be as serious as at first thought. The implicit assumption in Fig. 2 is that pores do not collapse on drying. Consider drying as assumed in Fig. 2b(ii), and additionally that an empty pore space collapses as water is removed. What remains within the pore are the two surface layers of water. The solid-like NMR signal will be unaffected. For this reason, a degree of credence can be applied to the pore size analysis. This would not be the case for drying as suggested in Fig. 2b(i), but then we do not assume this mode of drying.

To conclude this section, we note that both carbonation and microstructural damage may affect our data. However, the work to date has shown an important new way in which we may probe the microstructure of cement. With the caveats outlined, quantitative results have been obtained. It should be stressed that the total time required to acquire all the data presented in Fig. 5 is circa 6 weeks. This is for two reasons: first that the samples are equilibrated at each and every stage; and second that in order to resolve the changing gradients, a large number of water contents have been measured. Drying at constant relative humidity using salts was not thought to offer sufficiently refined drying to see the break in gradient, with only limited steps available, while using a humidity controlled environmental chamber was too resource intensive for initial work. Plans have been made to repeat the experiments using controlled drying in controlled humidity, CO_2 free environment.

6.3. NMR methodology

The method we have presented for pore size analysis of C–S–H in this work is distinct from previous measurements using either relaxation time analysis or (potentially) restricted NMR diffusometry. Most importantly, the new method is independent of knowing the surface relaxivity. However, the problem has shifted to one of fitting, and extrapolating to zero time, NMR signals. We have chosen an exponential form for the mobile signal component (which is likely uncontroversial) and a Gaussian for the solid component and have back extrapolated both their amplitudes to zero time using simple exponentials. Authors such as Powles and Strange [33] and Boden and Levine [34] have discussed the shape and echo time dependence of solid echoes for simple spin systems such as in crystalline gypsum. Empirically, for a complex structure such as cements the analysis is inapplicable and hence we have used the forms as discussed. Alternate forms yielded less good fits to the data.

7. Conclusion

We have presented an analysis of the porosity in white cement pastes based upon NMR signal amplitudes as a function of sample mass during controlled drying. The analysis has been interpreted in terms of water loss from two reservoirs of nanoscale planar pores that are suggested to be first the intra-C–S–H sheet pores and second the inter-C–S–H gel pores. The best estimates for the sheet- and gel pore thicknesses are 1.5 and 4.1 nm respectively. The ratio of the specific areas of the two pores types is estimated to be 2.4. The total volume ratio of the pore types is 0.88 whereas the volume ratio of readily

evaporable water within them is 0.63, implying that the sheet (sheet mobile water) porosity is 0.47 (0.38) of the total. The work has thrown light from a new perspective on the question of pore widths and total volumes. Further insight into the lateral extent of pores is forthcoming from double quantum filtered measurements being reported elsewhere [35].

Acknowledgements

The authors are grateful to the European Community under the Marie Curie Research Training Network MRTN-CT-2005-019283 "Fundamental understanding of cementitious materials for improved chemical physical and aesthetic performance" (http://www.nanocem.org/MC-RTN/) for the full support of AV. VR thanks the UK Physical Sciences and Engineering Research Council (EP/D037883/1) for funding. We thank Karen Scrivener, Ecole Polytechnique Federal de Lausanne for stimulating discussions and insight during the course of this work. We thank Robert Slade, University of Surrey, for help with differential scanning calorimetry assessment of carbonation.

References

[1] P.J. McDonald, M. Mitchell, M. Mulheron, Cement products: characterisation by NMR and MRI, Encyclopaedia of Materials: Science and Technology, Elsevier, 2005, pp. 1–9.
[2] J.-.P. Korb, NMR and nuclear spin relaxation of cement and concrete materials, Curr. Opin. Colloid Interface Sci. 14 (2009) 192–202.
[3] D.D. Lasic, J.M. Corbett, J. Jian, J.C. Mactavish, M.M. Pintar, R. Blinc, G. Lahajnar, NMR spin grouping in hydrating cement at 200 MHz, Cem. Concr. Res. 18 (1988) 649–653.
[4] D.D. Lasic, M.M. Pintar, R. Blinc, Are proton NMR observations supportive of the osmotic model of cement hydration, Philos. Mag. Lett. 58 (1988) 227–232.
[5] L. Miljkovic, D.D. Lasic, J.C. Mactavish, M.M. Pintar, R. Blinc, G. Lahajnar, NMR-studies of hydrating cement — a spin–spin relaxation study of the early hydration stage, Cem. Concr. Res. 18 (1988) 951–956.
[6] L. Miljkovic, J.C. Mactavish, J. Jian, M.M. Pintar, R. Blinc, G. Lahajnar, NMR-study of sluggish hydration of superplasticized white cement, Cem. Concr. Res. 16 (1986) 864–870.
[7] L.J. Schreiner, J.C. Mactavish, L. Miljković, M.M. Pintar, R. Blinc, G. Lahajnar, D. Lasic, L.W. Reeves, NMR line shape–spin–lattice relaxation correlation study of Portland-cement hydration, J. Am. Ceram. Soc. 68 (1985) 10–16.
[8] J. Greener, H. Peemoeller, C.H. Choi, R. Holly, E.J. Reardon, C.M. Hansson, M.M. Pintar, Monitoring of hydration of white cement paste with proton NMR, J. Am. Ceram. Soc. 83 (2000) 623–627.
[9] W.P. Halperin, J.-Y. Jehng, Y.-Q. Song, Application of spin–spin relaxation to measurement of surface area and pore size distributions in a hydrating cement paste, Magn. Reson. Imaging 12 (1994) 169–173.
[10] A.J. Bohris, U. Goerke, P.J. McDonald, M. Mulheron, B. Newling, B. Le Page, A broad line NMR and MRI study of water and water transport in Portland cement pastes, Magn. Reson. Imaging 16 (1998) 455–461.
[11] J.C. MacTavish, L. Miljkovic, H. Peemoeller, J.M. Corbett, J. Jian, D.D. Lasic, R. Blinc, G. Lahajnar, F. Milia, M.M. Pintar, Nuclear magnetic resonance study of hydration of synthetic white cement: continuous quantitative monitoring of water and Ca $(OH)_2$ during hydration, Adv. Cement Res. 8 (1996) 155–161.
[12] A. Plassais, M.P. Pomies, N. Lequeux, J.-P. Korb, D. Petit, F. Barberon, B. Bresson, Microstructure evolution of hydrated cement pastes, Phys. Rev. E 72 (2005) 041401.
[13] P.J. McDonald, J.-P. Korb, J. Mitchell, L. Monteilhet, Surface relaxation and chemical exchange in hydrating cement pastes: a two-dimensional NMR relaxation study, Phys. Rev., E 72 (2005) 011409.
[14] L. Monteilhet, J.-P. Korb, J. Mitchell, P.J. McDonald, A NMR T_2-store–T_2 2-dimensional correlation relaxation study of cement pastes, Phys. Rev. E 74 (2006) 061404.
[15] A. Valori, V. Rodin, P.J. McDonald, On the interpretation of ^{1}H 2D NMR relaxation exchange spectra in cements: is there exchange between pores with two characteristic sizes or Fe^{3+} concentrations? Cem. Concr. Res. 40 (2010) 1375–1377.
[16] K.R. Brownstein, C.E. Tarr, Importance of classical diffusion in NMR studies of water in biological cells, Phys. Rev. A 19 (1979) 2446–2453.
[17] F. D'Orazio, S. Bhattacharja, W.P. Halperin, K. Eguchi, T. Mizusaki, Molecular diffusion and nuclear-magnetic-resonance relaxation of water in unsaturated porous silica glass, Phys. Rev. B 42 (1990) 9810–9818.
[18] J.G. Powles, J.H. Strange, Zero time resolution nuclear magnetic resonance transients in solids, Proc. Phys. Soc. London 82 (1963) 6–15.
[19] H.M. Jennings, Refinements to colloid model of C–S–H in cement: CM-II, Cem. Concr. Res. 38 (2008) 275–289.
[20] R.F. Feldman, P.J. Sereda, A new model for hydrated Portland cement and its practical implications, Engin. J. 53 (1970) 53–59.
[21] www.nanocem.org; European Commission contract MRTN-CT-2005-019283, Nanocem.
[22] G.E. Pake, Nuclear resonance absorption in hydrated crystals: fine structure of the proton line, J. Chem. Phys. 16 (1948) 327–336.
[23] S. Meiboom, D. Gill, Modified spin-echo method for measuring nuclear relaxation times, Rev. Sci. Instrum. 29 (1958) 688–691.
[24] J. Israelachvili, Intermolecular and Surface Forces, 2nd ed.Academic Press, London, 1992.
[25] V. Kocaba, Personal communication, 2009.
[26] L.J. Parrot, A review of carbonation in reinforced concrete: Cement and Concrete Association, 1987.
[27] H. F. W. Taylor, Cement chemistry, 2nd ed.: Thomas Telford Publishing, London, 1997. (a) Section 7.3.3; (b) Section 7.4.4; (c) Section 8.2.4.
[28] T.C. Powers, T.L. Brownyard, Studies of the physical properties of hardened Portland cement paste, Bull. 22, Res. Lab. of Portland Cement Association, Skokie, IL, U.S.A., reprinted from J. Am. Concr. Inst. (Proc.), vol. 43 (1947). pp. 101–132, 249–336, 469–505, 549–602, 669–712, 845–880, 933–992.
[29] H.M. Jennings, A model for the microstructure of calcium silicate hydrate in cement paste, Cem. Concr. Res. 30 (2000) 101–116.
[30] A.J. Allen, J.J. Thomas, H.M. Jennings, Composition and density of nanoscale calcium-silicate-hydrate in cement, Nat. Mater. 6 (2007) 311–316.
[31] I.G. Richardson, The calcium silicate hydrates, Cem. Concr. Res. 38 (2008) 137–158.
[32] R.J.-M. Pellenq, A. Kushimac, R. Shahsavarib, K.J. Van Vlietd, M.J. Buehlerb, Y. Sidney, F.-J. Ulmb, A realistic molecular model of cement hydrates, PNAS 106 (2009) 16102–16107.
[33] J.G. Powles, J.H. Strange, Zero time resolution nuclear magnetic resonance transients in solids, Proc Phys. Soc. 82 (1963) 6–15.
[34] N. Boden, Y.K. Levine, R.T. Squires, NMR dipolar echoes in solids containing spin 1/2 pairs, Chem. Phys. Lett. 28 (1974) 523–525.
[35] A. Valori, Characterisation of cementitious materials by 1H NMR, PhD Thesis, University of Surrey, available at: http://www.nanocem.org/fileadmin/nanocem_files/documents/MC-RTN/Projects/Project_4/thesis_valori_final.pdf.